

# Discovery of Phospholipase D Inhibitors with Improved Drug-like Properties and Central Nervous System Penetration

Tricia L. May-Dracka, Fang Gao, Brian T. Hopkins, Xiaoping Hronowski, TeYu Chen, Jayanth V. Chodaparambil, Claire M. Metrick, Mike Cullivan, Istvan Enyedy, Maciej Kaliszczak, Mark W. Kankel, Isaac Marx, Mackenzie A. Michell-Robinson, Param Murugan, P. Rajesh Kumar, Michael Rooney, Eli Schuman, Anindya Sen, Ti Wang, Tao Ye, and Emily A. Peterson\*



Cite This: *ACS Med. Chem. Lett.* 2022, 13, 665–673



Read Online

ACCESS |



Metrics & More



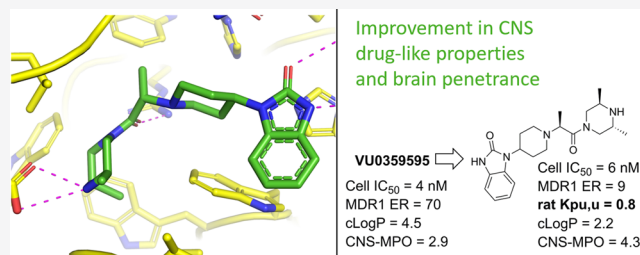
Article Recommendations



Supporting Information

**ABSTRACT:** Phospholipase D (PLD) is a phospholipase enzyme responsible for hydrolyzing phosphatidylcholine into the lipid signaling molecule, phosphatidic acid, and choline. From a therapeutic perspective, PLD has been implicated in human cancer progression as well as a target for neurodegenerative diseases, including Alzheimer's. Moreover, knockdown of PLD rescues the ALS phenotype in multiple *Drosophila* models of ALS (amyotrophic lateral sclerosis) and displays modest motor benefits in an SOD1 ALS mouse model. To further validate whether inhibiting PLD is beneficial for the treatment of ALS, a brain penetrant small molecule inhibitor with suitable PK properties to test in an ALS animal model is needed. Using a combination of ligand-based drug discovery and structure-based design, a dual PLD1/PLD2 inhibitor was discovered that is single digit nanomolar in the Calu-1 cell assay and has suitable PK properties for *in vivo* studies. To capture the *in vivo* measurement of PLD inhibition, a transphosphatidyltransferase pharmacodynamic LC-MS assay was developed, in which a dual PLD1/PLD2 inhibitor was found to reduce PLD activity by 15–20-fold.

**KEYWORDS:** Phospholipase D, PLD inhibitor, ALS, structure-based drug design, transphosphatidyltransferase



Amyotrophic lateral sclerosis (ALS) is a progressive and devastating neurodegenerative disease that affects motor neurons in the brain and spinal cord. ALS patients have gradual reduction in motor function, and most will advance to losing the ability to use their arms, walk, speak and breathe, succumbing to respiratory failure 2–5 years after disease onset.<sup>1</sup> In 2014, the Centers for Disease Control and Prevention approximated that ~16 000 people in the United States had ALS (1 in 20 000 persons).<sup>2</sup> There are no approved disease-modifying treatments for ALS. The quick progression of ALS coupled with no effective treatments underscores the high unmet need for the development of novel therapies.

ALS pathology can be classified into sporadic (sALS, no family history, 95% ALS patients) and familial (fALS, patients with a positive family history, 5% of ALS patients).<sup>3</sup> Over 25 different genes have been identified to contribute to the etiology of ALS; the SOD1 mutation and C9orf72 repeat expansion mutation are the most common genetic causes. Although recent discoveries have vastly improved our understanding of the different disease pathways in ALS, a deeper understanding of the complex genetic architecture is necessary to effectively identify novel druggable targets for disease modifying therapies.

To discover and evaluate new targets for the treatment of ALS, a genome-wide screen was conducted to discover potential modifiers of *Drosophila* models of degenerative eye phenotypes associated with the expression of human FUS transgenes carrying fALS mutations.<sup>4</sup> After cross-referencing the findings from the *Drosophila* screen with postmortem gene expression in motor neurons from sALS patients,<sup>5</sup> several genes were implicated, including three that are components of the phospholipase D pathway (ARFGAP3, RALB, and PLD).<sup>4</sup> Phospholipase D (PLD) is a phospholipase enzyme responsible for hydrolyzing phosphatidylcholine into the lipid signaling molecule, phosphatidic acid (PA), and choline.<sup>6</sup> PA is a critical lipid constituent in cell membranes; c-Raf and mTOR directly bind PA to mediate translocation or activation, respectively.<sup>7</sup> PA also has been associated with a variety of

**Received:** December 18, 2021

**Accepted:** March 1, 2022

**Published:** March 3, 2022



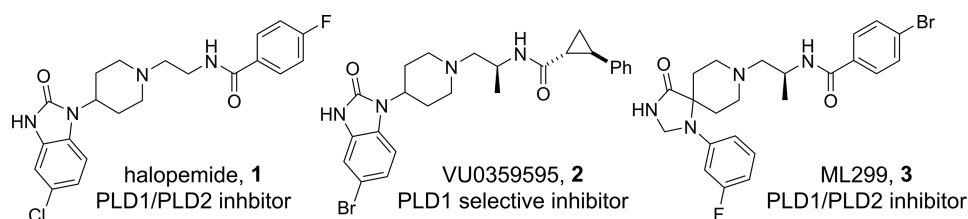


Figure 1. Known PLD inhibitors.

signaling cascades involving cell growth, proliferation and survival.<sup>8</sup>

Historical interest in PLD as a target for therapeutic intervention for oncology had resulted in the identification of several published PLD inhibitors.<sup>9</sup> One of the first reported PLD inhibitors was derived from halopemide (1, Figure 1), a D2 antagonist and moderate PLD1/PLD2 dual inhibitor which inspired the discovery by Novartis that potency for PLD2 inhibition could be increased by replacing the fluorophenyl amide with bicyclic heterocycles such as indole (not pictured).<sup>10</sup> Capitalizing on this discovery, Lindsley and co-workers further advanced the halopemide scaffold to deliver isoform selective inhibitors VU0359595 (2), and the triaza-spirocyclic scaffold ML299 (3), that could be modulated to afford PLD2 or dual PLD1/PLD2 inhibition (Figure 1).<sup>11</sup> These molecules exhibited reasonable *in vitro* potency but unfortunately were substrates for efflux transporter P-glycoprotein (Pgp) with efflux ratios (ER) in the MDCK-MDR1 assay > 40 and a correspondingly low ratio of unbound brain/unbound plasma concentration ( $K_{pu,u}$ ).<sup>12</sup> These absorption, distribution, metabolism, and elimination (ADME) properties rendered these tool inhibitors unsuitable for use in evaluating the effect of PLD inhibition in mouse models of ALS, due to their inability to achieve sufficient free brain concentrations.

In the absence of either the PLD1 or PLD2 human crystal structures to guide structure-based drug design,<sup>13</sup> a ligand-based drug design approach was pursued, starting from the reported PLD1-selective<sup>14</sup> inhibitors, while in parallel conducting an HTS campaign. The strategic decision to focus on the PLD1-selective inhibitors was predicated on the original *Drosophila* findings, which identified a number of PLD1 specific pathway proteins as genetic suppressors of ALS-related phenotypes.<sup>4</sup> It is important to note that *Drosophila* contains a single PLD gene and thus it was unclear from the outset whether inhibition of both isoforms in humans would be desired.<sup>4</sup> To further our understanding of the structure–activity relationship (SAR) for driving the potency against PLD1 and PLD2, all new analogues synthesized were screened against both isoforms. The enzymatic activity of inhibitors was assessed by immunoprecipitation of PLD1 or PLD2 from HEK-293 cell lysates (referred to as IPoP) and cellular inhibition was measured as previously described in Calu-1 cells.<sup>15,16</sup>

With the goal to design inhibitors that exhibited good blood-brain barrier (BBB) permeability, the team focused on synthesizing molecules with a minimal number of hydrogen-bond (H-bond) donors as a means to reduce recognition by Pgp (also known as MDR1, Table 1).<sup>17</sup> Building from leads disclosed by the Lindsley group, the benzimidazolone compound 4, which demonstrated good biochemical (PLD1  $IC_{50}$  = 33 nM) and cellular (Calu  $IC_{50}$  = 16 nM) potency and human liver microsomal stability (HLM  $Cl_{int}$  <4 mL/min/

Table 1. Modification of the Benzimidazolone

Cmpd	A/B ring	PLD1/PLD2 $IC_{50}$ ( $\mu$ M) <sup>a</sup>	Calu-1 $IC_{50}$ ( $\mu$ M) <sup>b</sup>	HLM / RLM (mL/min/kg) <sup>c</sup>	MDR1 ER <sup>d</sup>
4		0.033 / 5.6	0.016	<4 / 170	82
5		9.3 / >10	>10	23 / 314	2.0
6		1.2 / >10	1.1	42 / 311	8.0
7		>10 / >10	>10	<4 / 16	7.7
8		0.97 / >10	4.2	42 / 311	8.0

<sup>a</sup>Biochemical inhibition of PLD1/2 was determined by immunoprecipitated on plate (IPoP) assay of PLD1/2 from HEK cells. <sup>b</sup>Cellular assay performed in Calu-1 cells. <sup>c</sup>Intrinsic Cl ( $Cl_{int}$ ) in rat or human liver microsomes. <sup>d</sup>Efflux ratio =  $P_{app}(B - A) / P_{app}(A - B)$  MDCK-MDR1.

kg), was deemed a suitable scaffold for optimization with the objective of improving the central nervous system (CNS) drug-like properties (Table 1, entry 1). Analogue 4 suffered from high *in vivo* clearance (rat IV CL = 69 mL/min/kg) and significant MDR1-mediated efflux (ER = 82), which correlated with low unbound brain exposure ( $K_{pu,u}$  = 0.02) when dosed in a rat infusion model. Several analogues were prepared with the aim of replacing the H-bond donor on the benzimidazolone ring. Methylation of the benzimidazolone nitrogen resulted in a complete loss of PLD potency and still maintained an unacceptable MDR1 efflux ratio of 19. Replacement of the benzimidazolone with the benzoxazolone moiety led to 5, which was a weak Pgp substrate (ER = 2.0); however, both

benzoxazolone **5** and the indolinone **6** analogues resulted in a significant loss in PLD1 biochemical potency. Removal of the aryl motif while maintaining the cyclic urea in **7** demonstrated no inhibition at the highest concentration. Notably, this was one of the first modifications which demonstrated an improvement in the *in vitro* rat liver microsomes assay (RLM  $CL_{int} = 16$  mL/min/kg). To probe the role of the carbonyl functionality, the benzimidazolidinone was replaced with the indazole in **8**, but this also resulted in a decrease in potency (Table 1). These findings indicated that the carbonyl, NH bond donor, and aromatic ring within the benzimidazolone moiety were essential components of the pharmacophore required for PLD affinity.

A cocrystal structure of compound **4** bound to hPLD2<sup>18</sup> was obtained at 2.9 Å resolution (Figure 2). The structure revealed

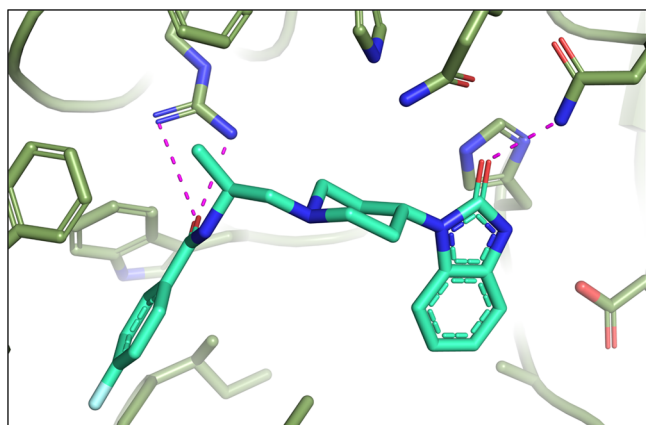


Figure 2. X-ray cocrystal of **4** with PLD2 (PDB# 6OHQ)

the benzimidazolone moiety formed interactions with residues Gln642 and Asn773 within the HKD pocket. The piperidine linker orients the benzylamide moiety into a region of the

active site where an electrostatic interaction occurs between the carbonyl of the benzylamide moiety and Arg486.

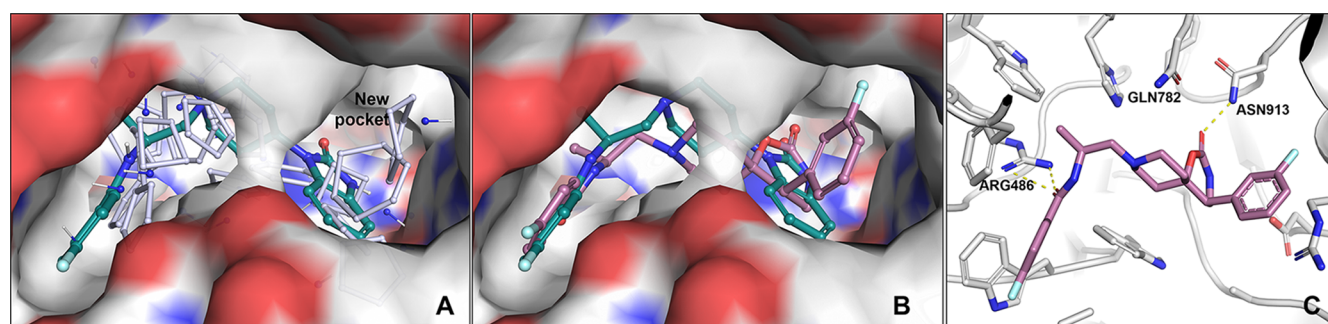
Having confirmed the carbonyl, NH bond and aromatic moieties were necessary to achieve inhibition of PLD1, a series of analogues were designed composed of novel spirocyclic cores, which maintained the putative pharmacophore while facilitating modulation of the physicochemical properties via increased Fsp<sup>3</sup> character.<sup>19</sup> This effort initiated from the dual PLD1/PLD2 inhibitor ML299 (**3**, Table 2, entry 1), which also demonstrated high Pgp ER and ADME properties that made it unsuitable as an *in vivo* CNS tool. Exploration of fused spirocyclic replacements for the imidazolidin-4-one moiety present in ML299 (**3**) provided several inhibitors with improved ER and microsomal stability as outlined in Table 2. The 3,4-dihydroquinolin-2-one **9** resulted in an improvement in the *in vivo* CL (rat IV CL = 8.6 mL/min/kg), although compound **9** was a Pgp substrate (MDCK-MDR1 ER = 11) with a low  $K_{pu,u}$  (0.02 in rat). Similarly, spirocyclic ureas **10** and **11** did not improve activity against PLD1 and, as expected, increased ER. Interestingly, the spirocyclic carbonate **12** restored the activity against PLD1 and demonstrated moderate *in vivo* clearance that warranted further investigation of the SAR around the fused aromatic ring. Introducing a fluorine substituent on the aryl motif led to **13**, which exhibited similar PLD biochemical and Calu-1 cellular potency but was less stable in liver microsomes compared to the des-fluoro analogue **12**. However, replacing the phenyl moiety with the pyridooxazinones (**14** and **15**) maintained inhibition of PLD1 and improved microsomal stability. Unfortunately, this improved *in vitro* stability was not reflected *in vivo*. One exciting discovery culminating from this effort was the design of **16**, which was based on *in silico* solvent mapping of the PLD2 active site that revealed a novel pocket adjacent to the HKD binding domain into which it was hypothesized that substituents attached at C5 would project (Figure 3A). This new chemical series demonstrated drastically improved PLD1/2 potency and, more importantly, enabled the first X-ray

Table 2. Exploration of Novel Spirocyclic Cores

Cmpd	<b>3</b>	<b>9</b>	<b>10</b>	<b>11</b>	<b>12</b>	<b>13</b>	<b>14</b>	<b>15</b>	<b>16</b>
	ML299								
PLD1 IC <sub>50</sub> (μM) <sup>a</sup>	0.049	0.49	0.28	>10	0.066	0.071	0.11	0.20	0.022
PLD2 IC <sub>50</sub> (μM) <sup>a</sup>	0.067	>10	>10	>10	1.3	1.0	3.2	4.1	0.064
Calu-1 IC <sub>50</sub> (μM) <sup>b</sup>	0.010	0.46	0.72	>10	0.074	0.078	0.078	0.054	0.002
HLM / RLM (mL/min/kg) <sup>c</sup>	89 / 312	28 / 83	14 / 66	39 / 113	39 / 103	68 / 250	12 / 50	13 / 48	38 / 394
MDR1 ER <sup>d</sup>	40	11	67	93	218	42	47	68	12
Solubility (μg/mL) <sup>e</sup>	3.8	59	51	71	76	nd	58	59	61
Rat IV CL [CLu](mL/min/kg) <sup>f</sup>	36 [>3800]	8.6 [42]	15 [74]	nd	40 [172]	nd	48 [69]	40 [83]	119 [308]

<sup>a</sup>Biochemical inhibition of PLD1/2 was determined by immunoprecipitation on a plate (IPoP) of PLD1/2 from HEK cells. <sup>b</sup>Cellular assay performed with Calu-1 cell line. <sup>c</sup>Intrinsic CL ( $CL_{int}$ ) in rat or human liver microsomes. <sup>d</sup>Efflux ratio =  $P_{app}(B - A) / P_{app}(A - B)$  in MDR1-MDCK. <sup>e</sup>Kinetic solubility pH = 6.8. <sup>f</sup>Clearance determined by cassette dosing; Clu = unbound *in vivo* clearance (Cl/fu).





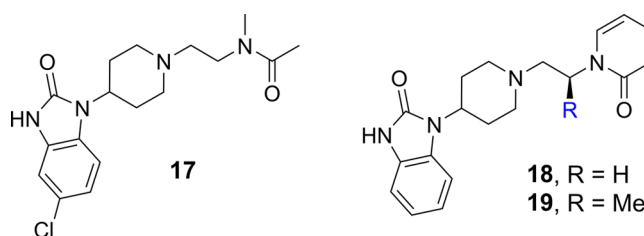
**Figure 3.** (A) Solvent mapping of the PLD2 active site; (B) docking of inhibitor **16** into X-ray cocrystal of PLD2 with inhibitor **4** showing C5 substituent filling pocket adjacent to benzimidazolinone ring; (C) X-ray cocrystal structure of **16** with PLD1b (PDB# 6OHR).

cocrystal structure of PLD1 (Figure 3C).<sup>18</sup> Despite **16** achieving a 5-fold increase in cellular potency compared to ML299 (**3**), **16** and related analogues continued to demonstrate inadequate ADME and CNS properties, leading to the deprioritization of this scaffold. The cocrystal structure of **16** bound to PLD1b revealed subtle differences in the binding mode within the active site (Figure 2 vs Figure 3C). Compound **16** maintained the key binding interactions with conserved residues Gln782 and Asn913 (in the HKD pocket, PLD1b numbering), which oriented the C5 fluorophenyl ring to bind in the cavity newly identified from the PLD2 solvent mapping, and Arg464/486 (PLD2/PLD1b) with the amide carbonyl. Comparison of the D-ring phenyl amide binding pocket and the space occupied by the alpha-methyl alkyl linkers led to observations that rationalized the isoform selectivity differences observed for reported PLD inhibitors, which are described in detail in ref 18.

Utilizing insights gained from the hPLD1 cocrystal structure, a series of compounds were designed to further interrogate the pharmacophore required for binding in the phenyl amide (D-ring) region of the structure. Since the spirocyclic carbonate series had exhibited poor ADME properties, all further optimization was performed using the original benzimidazolinone series. To reduce the MW and lipophilicity, more truncated analogues were prepared to establish the minimum pharmacophore. The *N*-methylacetamide analogue **17**, which was designed to maintain the electrostatic interaction with Arg486 but eliminate the amide H-bond and lipophilic phenyl moiety, maintained good PLD1 and Calu-1 cellular inhibition while retaining selectivity over PLD2 (Table 3). Despite the high CNS-MPO score for **17** and superior drug-like properties that provided improved stability in HLM, these changes did not ultimately result in a reduction of Pgp-mediated efflux. Having demonstrated that the H-bond donor was not required for activity, pyridone **18** was synthesized, which was designed to maintain interaction with Arg486, but also to determine if potency could be improved by reintroduction of an aromatic ring. Interestingly, the biochemical potency was not impacted, although inhibition of Calu-1 was diminished. It was observed that introducing conformational constraint on the alkyl linker via the (*S*)-methyl substitution (**19**) improved the potency and reduced the ER value, although this improvement did not translate to an improved  $K_{p,u}$  (0.02 in rat). Further exploration of scaffold **19** by introduction of electron-withdrawing groups on the pyridone (data not shown) was not effective in improving PLD inhibition or further reducing the ER.

Inspired by the observation that both the phenyl (D ring) and the N–H amide moieties were not required for PLD1

**Table 3. Removal of the Amide H-Bond**

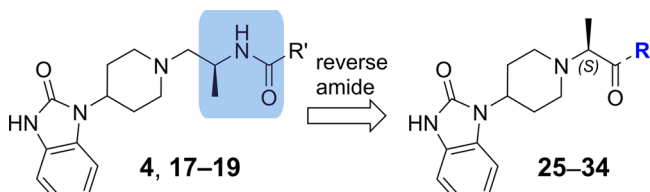


compd	IC <sub>50</sub> (μM)			MDR1 ER <sup>c</sup>	cLogP/MPO <sup>d</sup>
	PLD1 <sup>a</sup>	PLD2 <sup>a</sup>	Calu-1 <sup>b</sup>		
<b>17</b>	0.13	>10	0.18	24	2.3/5.8
<b>18</b>	0.12	>10	0.98	17	1.6/5.8
<b>19</b>	0.043	>10	0.058	8.6	1.8/5.8

<sup>a</sup>Biochemical inhibition of PLD1/2 was determined by immunoprecipitation on a plate (IPoP) of PLD1/2 from HEK cells. <sup>b</sup>Cellular assay performed with Calu-1 cell line. <sup>c</sup>Rat or human liver microsomes. <sup>d</sup>Efflux ratio determined by measuring Papp(B-A)/Papp(A-B) in MDR1-MDCK.

activity, exploration of the linkage between the piperidine C ring and the amide carbonyl was pursued. Comparison of X-ray structures of spirocyclic inhibitor **3** and benzimidazolinone **4**, which exhibit differences between the two carbonyls forming key interactions with the protein (HKD and Arg464), led us to speculate that the Arg464 side chain was flexible and could reorient to maintain the critical electrostatic interaction with the amide carbonyl moiety.<sup>18</sup> To test this hypothesis, a series of structurally distinct analogues were designed containing an alanine linker, which reversed the amide linkage compared to previously prepared analogues and positioned the carbonyl closer to the piperidine ring (Table 4). Based on the docking studies, it was perceived that introducing the *S*-Me alpha substituent would rigidify the molecule, directing the carbonyl moiety toward the side chain of Arg464. Since this alanine linkage was anticipated to yield a novel pharmacophore that was amenable for parallel medicinal chemistry (PMC), a library of analogues was enumerated utilizing *in silico* docking studies to identify amine fragments predicted to bind in this region of the protein and would improve the drug-like properties with respect to reducing the molecular weight, Fsp<sup>2</sup> character and lipophilicity. Utilizing the commercially available 1-(piperidin-4-yl)-1,3-dihydro-2*H*-benzimidazol-2-one starting material **20**, the piperidine amine was alkylated, affording the ester **22**, which was separated by SFC to obtain enantioenriched **23**, which was saponified to provide **24** in 98% yield. The acid intermediate **24** underwent HATU-

Table 4. SAR of Truncated, Reversed Amides

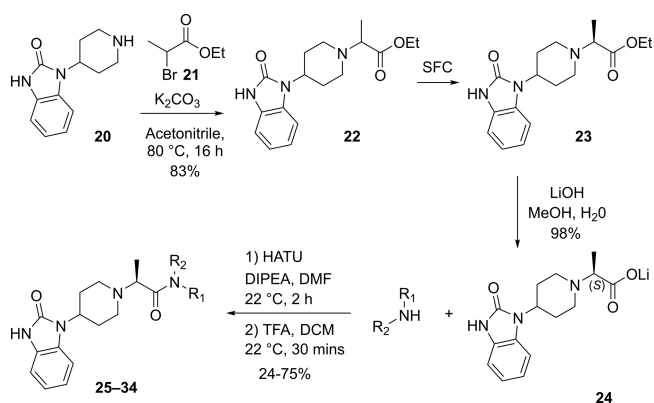


Cmpd	R	PLD1 / PLD2 IC <sub>50</sub> (μM) <sup>a</sup>	Calu-1 IC <sub>50</sub> (μM) <sup>b</sup>	HLM / RLM (mL/min/kg) <sup>c</sup>	MDR1/ BCRP ER <sup>d</sup>	Rat IV CL [Clu] (mL/min/kg) <sup>e</sup>
25		0.17 / 2.9	1.2	10 / >300	25 1.2	34 [192]
26		0.10 / 0.32	0.006	>200 / >300	22	nd
27		0.38 / >10	0.56	<5 / 162	36 1.5	13 [ND]
28		0.076 / 1.1	0.16	<5 / <10	5.5 2.3	39 [73]
29		0.32 / nd	0.19	<5 / 29	13	39 [73]
30		0.36 / 7.0	0.28	8 / 56	5.2	39 [73]
31		0.068 / 0.92	0.044	<4 / 59	50	nd
32		0.14 / nd	0.18	12 / 84	5.4	nd
33		0.040 / 0.20	0.032	6.9 / 43	14	45 [68]
34		0.044 / 0.23	0.006	6.0 / 64	9.2 1.2	28 [84]

<sup>a</sup>Biochemical inhibition of PLD1/2 was determined by immunoprecipitation on a plate (IPoP) of PLD1/2 from HEK cells. <sup>b</sup>Cellular assay performed with Calu-1 cell line. <sup>c</sup>Rat or human liver microsomes. <sup>d</sup>Efflux ratio determined by measuring  $P_{app}(B-A)/P_{app}(A-B)$ . <sup>e</sup>cassette dosing used; [Clu] = Unbound clearance ( $Cl/f_u$ ).

mediated amide coupling to deliver a focused library of novel alanine linker analogues (Scheme 1). Several surprising hits emerged from the library. SAR studies conducted on the amide moiety using the linker contained in compounds 1–19 showed a clear preference for the presence of an aromatic ring to fill the hydrophobic pocket defined by residues W364 and W365, L407, I409, and W519.<sup>18</sup> As postulated by comparison of the PLD1 and PLD2 Xray structures, the presence of an aromatic ring that can engage in a  $\pi$ -stacking interaction with W519 imparts greater potency against PLD2, while truncated Sp<sup>3</sup> rings demonstrated improved inhibition of PLD1 (compare 26 and 28). The observed potency and lower ER obtained by analogues containing a basic amine moiety in place of a more lipophilic aromatic substituent was surprising. The increased potency on PLD2 without the aromatic ring for  $\pi$ -stacking supports the hypothesis described in ref 18, that the distance between the benzimidazolone and the chiral methyl group present on the linker is key in obtaining PLD1 selectivity, and

## Scheme 1. Synthesis of Truncated, Reversed-Amide Containing Benzimidazolines 25–34



that compounds with a smaller distance between these two moieties can be accommodated by both PLD1 and PLD2 isoforms. Comparison of morpholine 27 with piperazine 28 shows an increase in potency with the inclusion of the NH, and piperazine analogues containing substitution on that nitrogen were not tolerated, pointing to the possibility of a new favorable interaction with the protein. Piperazine 28 showed modestly improved  $K_{pu,u} = 0.14$  compared to previous analogues tested. Exploration of substitution around the piperazine ring revealed a preference for 3,5-dimethyl substitution, with the 3S,5S-stereochemistry (34) demonstrating superior potency in the Calu-1 cellular assay. A cocrystal structure of 34 was obtained with PLD2 and as anticipated, a new interaction with the protein was identified, with the piperazine amine forming an H-bonding interaction with Asp518 (Figure 4A). The axial piperazine methyl group is accommodated in a hydrophobic pocket bordered by Ile411 and Trps364/365. Also present in the cocrystal structure with 34 is a water molecule that forms a bridging interaction between the benzimidazolone NH and Glu786 and Asp784, which provides rationale for the required H-bond donor at that position. Also of note is the movement of Leu514, where the alanine methyl present in 34 has a different trajectory than the methyl present on the linker in PLD1-preferring inhibitor 4 (Figure 4B) an observation in line with our previously reported hypothesis on the structural basis of isoform selectivity.<sup>18</sup> A more intriguing discovery was the improvement in the CNS penetration observed for inhibitor 34, which demonstrated a  $K_{pu,u} = 0.8$  in a rat infusion model. Further profiling of compound 34 demonstrated no BCRP efflux, hERG liability, or inhibition of CYP enzymes.<sup>20</sup> The ADME properties and potency of analogue 34 prompted the team to move forward with this compound to explore the measurement of PLD inhibition *in vivo*.

With the discovery of compound 34, which had the potency and ADME properties suitable for use as an *in vivo* tool, the team set about developing a PLD dependent pharmacodynamic assay for determining a PK/PD relationship for 34. Unfortunately, utilizing phosphatidic acid (PA) as a direct readout of PLD activity was deemed impractical, owing to its short *in vivo* half-life and existence of multiple pathways, including PLD, which contribute to the formation of phosphatidic acid.<sup>21</sup> Therefore, an alternative approach was adopted, wherein PLD activity was correlated with its ability to catalyze a transphosphatidylation reaction of phosphatidyl choline (PC) with short-chain primary alcohols, such as

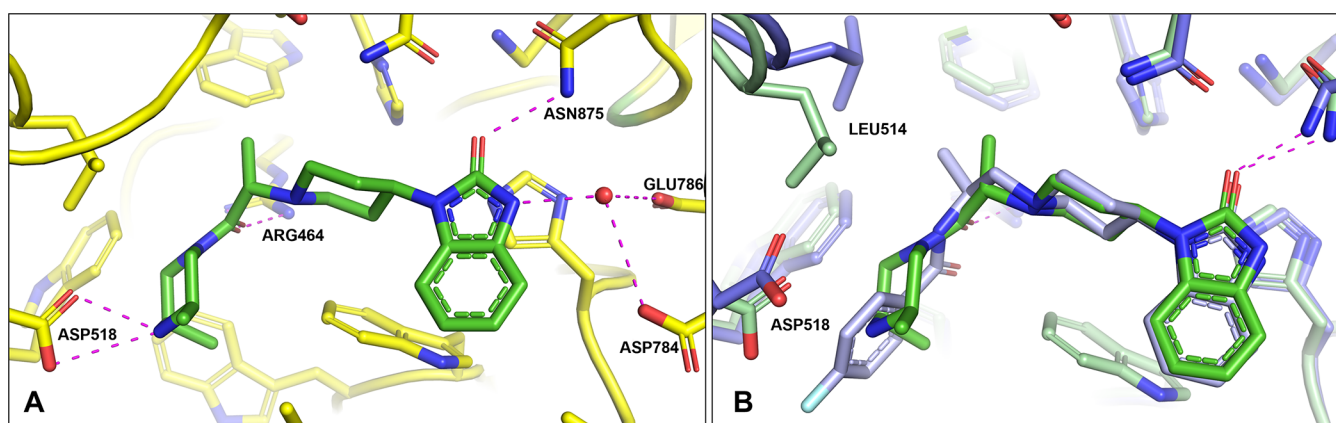


Figure 4. (A) X-ray cocrystal of **34** with hPLD2 (PDB# 7SVP); (B) overlay of X-ray cocrystals of **4** (slate) and **34** (green) in hPLD2.

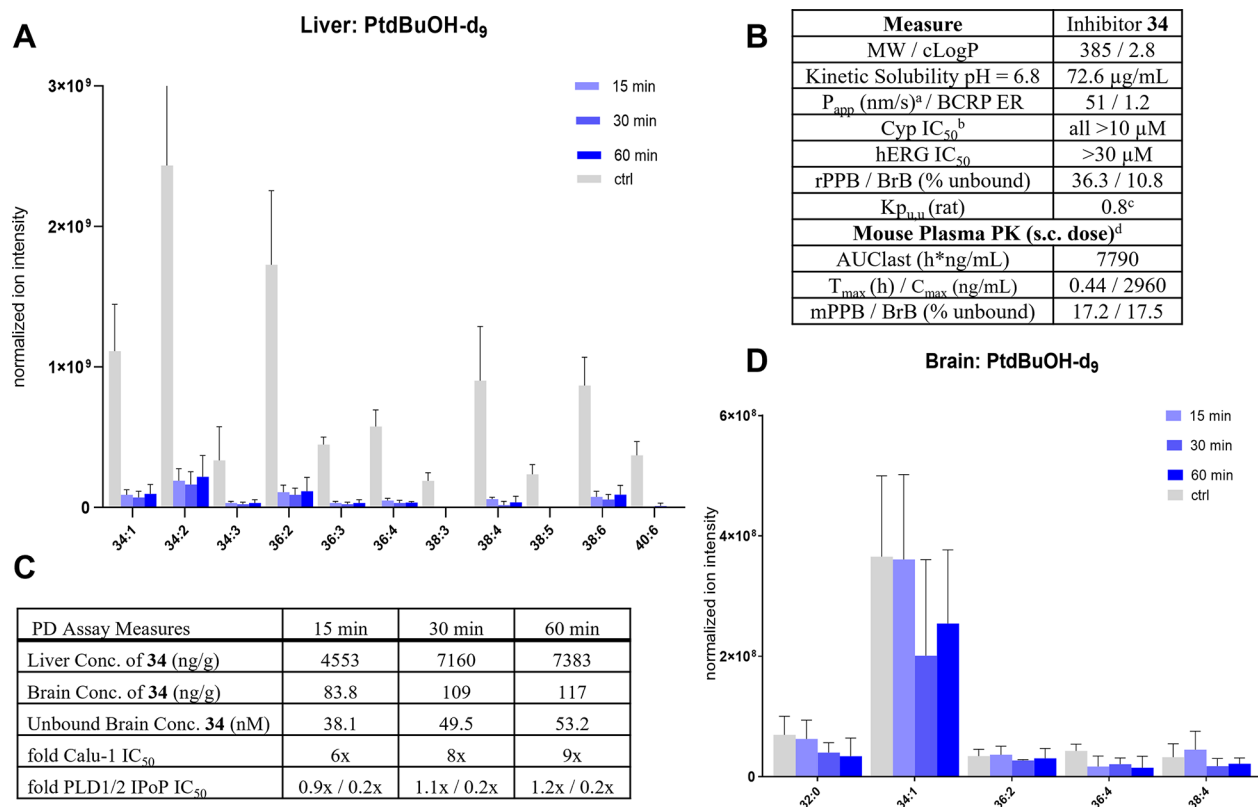


Figure 5. Expanded profile of PLD inhibitor **34** and measurement of *in vivo* PLD inhibition in mice treated with **34**. (A) Reduction of various PtdBuOH- $d_9$  species by **34** in liver. (B) Selectivity and rodent PK of **34**. <sup>a</sup>Average of A-B/B-A Papp in MDCK cells with low MDR1 expression. <sup>b</sup>CYPs evaluated: 1A2, 2B6, 2D6, 2C9, 2C19, 3A4. <sup>c</sup>Average of two experiments with  $n = 3$  rats each. <sup>d</sup>Formulation: HPMC/Tween. (C) Liver/brain concentrations of **34** at measured time points. (D) PtdBuOH- $d_9$  species in brains of mice treated with **34**.

ethanol or 1-butanol to yield phosphatidylethanol (PtdEtOH) or phosphatidylbutanol (PtdButOH). The transphosphatidylation reaction is exclusive to phospholipase D1/D2 and has been employed as a specific assay for assessing the enzyme activity in cells such as the Calu-1 assay and *in vivo*.<sup>22,23</sup> Using LC-MS detection, PtdButOH(34:1) was confirmed to exhibit significantly higher intensity than PtdEtOH(34:1) (data not shown), therefore 1-butanol was selected for further experiments and, based on the enhanced signal sensitivity, deuterated 1-butanol- $d_{10}$  was employed to improve assay specificity.<sup>24</sup>

An extensive *in vivo* optimization effort was necessary for establishing a time-course and concentration effect for the transphosphatidylation (PtdBut- $d_9$ ) readout with respect to  $t$ -

butanol- $d_{10}$  to ensure maximum signal/noise ratio. These experiments determined that the optimal detection period following injection of  $t$ -butanol- $d_{10}$  was 15 min, as (PtdBut- $d_9$ ) levels in liver and brain declined significantly at 30 min. Using an unbiased LC-FTICR-MS assay, 18 unique phosphatidylbutanol- $d_9$  (PtdBut- $d_9$ ) species were detected from the liver and seven from the brain. The most abundant PtdBut- $d_9$  species from the brain and the liver were different, with PtdBut- $d_9$  (34:1) proving to be most abundant in the brain and PtdBut- $d_9$  (34:2) in the liver (Figure 5).

Although **34** exhibited moderate oral bioavailability (%F = 21) when dosed orally in rat, the lengthy oral absorption profile ( $T_{\text{max}} = 3$  h) was considered impractical for the PD



assay. Subcutaneous (SC) dosing of **34** in mice resulted in a shorter  $T_{max}$ , 0.4 h, indicating that measurement of transphosphatidylolation within 1 h of dosing compound would be possible. To understand the time course of PLD inhibition *in vivo* with **34**, mice were first dosed subcutaneously with **34** (10 mg/kg) at 15, 30, and 60 min prior to injection with 1-butanol- $d_{10}$  and tissues were collected after 15 min. Comparison of compound-treated and control mice revealed that 16 out of 18 PtdBut- $d_9$  species in the liver showed statistically significant decreases, with only two low-abundance lipids not showing a meaningful signal ( $p < 0.05$ , Figure 5A). In contrast to the excellent  $K_{pu,u}$  observed in the rat infusion experiment, **34** did not show expected brain concentrations in the mice at the selected time-points and thus minimal changes were observed in the production of PtdBut- $d_9$  species in the brain (Figure 5D). The  $K_{pu,u}$  of **34** in mouse at all three time points was 0.02, providing a maximum of 9× coverage of the Calu-1  $IC_{50}$ . In the liver, there was robust inhibition, but minimal difference between the 15, 30, or 60 min time points, presumably due to the large multiple over  $IC_{50}$  observed in the liver at all time points (Figure 5C). While not statistically significant, the later time points in the brain samples, which correlated with higher exposure, did show a trend toward lowering of PtdBut- $d_9$  (34:1).

Starting from reported peripherally restricted PLD inhibitors, we identified brain penetrant PLD inhibitor **34** with improved drug-like attributes and ADME properties. Through this effort, the first cocrystal structures of human PLD1 and PLD2 isoforms were characterized and the SAR rationale for isozyme selectivity was uncovered. While **34** showed excellent brain penetration in rats, the initial PD experiment in mice with PLD1/2 inhibitor **34** failed to show a significant reduction in PLD-mediated transphosphatidylolation in the brain tissue, likely due to the reduced brain exposure of **34** in mice vs rats at the measured time point. The observed difference in the  $K_{pu,u}$  values between the mouse PD and the rat IV infusion  $K_{pu,u}$  measurement may be attributed to the SC dosing in mouse and measurement at non-steady-state conditions. Additional experiments are required to determine an *in vivo* PK/PD correlation and establish which of the *in vitro* potency readouts are predictive for the observed *in vivo* pharmacodynamic effect necessary for guiding any future medicinal chemistry effort. While the neuroPK observed in mice was disappointing, compound **34** does exhibit sufficient potency, ADME properties, and BBB permeability in rat to serve as a tool CNS-penetrant compound for evaluating PLD signaling *in vivo*. More importantly, discovery of the H-bond interaction between **34** and ASP518 (PLD2) should facilitate the discovery and optimization of future PLD inhibitors.

## ■ ASSOCIATED CONTENT

### SI Supporting Information

The Supporting Information is available free of charge at <https://pubs.acs.org/doi/10.1021/acsmmedchemlett.1c00682>.

Compound synthesis preparation, characterization data, and X-ray crystallography data (PDF)

## ■ AUTHOR INFORMATION

### Corresponding Author

Emily A. Peterson – Biotherapeutic and Medicinal Sciences, Biogen, Cambridge, Massachusetts 02142, United States;

[orcid.org/0000-0001-5854-2505](https://orcid.org/0000-0001-5854-2505);

Email: [emily.peterson@biogen.com](mailto:emily.peterson@biogen.com)

## Authors

- Tricia L. May-Dracka – Biotherapeutic and Medicinal Sciences, Biogen, Cambridge, Massachusetts 02142, United States
- Fang Gao – Biotherapeutic and Medicinal Sciences, Biogen, Cambridge, Massachusetts 02142, United States
- Brian T. Hopkins – Biotherapeutic and Medicinal Sciences, Biogen, Cambridge, Massachusetts 02142, United States; [orcid.org/0000-0002-2912-9954](https://orcid.org/0000-0002-2912-9954)
- Xiaoping Hronowski – Biotherapeutic and Medicinal Sciences, Biogen, Cambridge, Massachusetts 02142, United States; [orcid.org/0000-0002-8556-4336](https://orcid.org/0000-0002-8556-4336)
- TeYu Chen – Biotherapeutic and Medicinal Sciences, Biogen, Cambridge, Massachusetts 02142, United States
- Jayanth V. Chodaparambil – Biotherapeutic and Medicinal Sciences, Biogen, Cambridge, Massachusetts 02142, United States
- Claire M. Metrick – Biotherapeutic and Medicinal Sciences, Biogen, Cambridge, Massachusetts 02142, United States
- Mike Cullivan – Biotherapeutic and Medicinal Sciences, Biogen, Cambridge, Massachusetts 02142, United States
- Istvan Enyedy – Biotherapeutic and Medicinal Sciences, Biogen, Cambridge, Massachusetts 02142, United States; [orcid.org/0000-0001-9864-6018](https://orcid.org/0000-0001-9864-6018)
- Maciej Kaliszczak – Research and Early Development Biomarkers, Biogen, Cambridge, Massachusetts 02142, United States
- Mark W. Kankel – Neuromuscular & Movement Disorders Research Unit, Biogen, Cambridge, Massachusetts 02142, United States
- Isaac Marx – Biotherapeutic and Medicinal Sciences, Biogen, Cambridge, Massachusetts 02142, United States; [orcid.org/0000-0003-2393-5768](https://orcid.org/0000-0003-2393-5768)
- Mackenzie A. Michell-Robinson – Neuromuscular & Movement Disorders Research Unit, Biogen, Cambridge, Massachusetts 02142, United States
- Param Murugan – Biotherapeutic and Medicinal Sciences, Biogen, Cambridge, Massachusetts 02142, United States
- P. Rajesh Kumar – Biotherapeutic and Medicinal Sciences, Biogen, Cambridge, Massachusetts 02142, United States
- Michael Rooney – Biotherapeutic and Medicinal Sciences, Biogen, Cambridge, Massachusetts 02142, United States
- Eli Schuman – Biotherapeutic and Medicinal Sciences, Biogen, Cambridge, Massachusetts 02142, United States
- Anindya Sen – Neuromuscular & Movement Disorders Research Unit, Biogen, Cambridge, Massachusetts 02142, United States
- Ti Wang – Biotherapeutic and Medicinal Sciences, Biogen, Cambridge, Massachusetts 02142, United States
- Tao Ye – Research and Early Development Biomarkers, Biogen, Cambridge, Massachusetts 02142, United States

Complete contact information is available at: <https://pubs.acs.org/doi/10.1021/acsmmedchemlett.1c00682>

## Notes

The authors declare no competing financial interest.

## REFERENCES

- (1) van Es, M. A.; Hardiman, O.; Chio, A.; Al-Chalabi, A.; Pasterkamp, R. J.; Veldink, J. H.; van den Berg, L. H. Amyotrophic Lateral Sclerosis. *Lancet* **2017**, *390*, 2084–2098.
- (2) Mehta, P.; Kaye, W.; Raymond, J.; Wu, R.; Larson, T.; Punjani, R.; Heller, D.; Cohen, J.; Peters, T.; Muravov, O.; Horton, K. Prevalence of Amyotrophic Lateral Sclerosis. *MMWR Morb. Mortal. Wkly. Rep.* **2018**, *67*, 216–218.
- (3) Nguyen, H. P.; Van Broeckhoven, C.; van der Zee, J. ALS Genes in the Genomic Era and their Implications for FTD. *Trends Genet* **2018**, *34*, 404–423.
- (4) Kankel, M. W.; Sen, A.; Lu, L.; Theodorou, M.; Dimlich, D. N.; McCampbell, A.; Henderson, C. E.; Shneider, N. A.; Artavanis-Tsakonas, S. Amyotrophic Lateral Sclerosis modifiers in *Drosophila* reveal the Phospholipase D pathway as a potential therapeutic target. *Genetics* **2020**, *215*, 747–766.
- (5) (a) Kaplan, A.; Spiller, K. J.; Towne, C.; Kanning, K. C.; Choe, G. T.; Geber, A.; Akay, T.; Aebischer, P.; Henderson, C. E. Transplantation of Neural Precursors Derived from Induced Pluripotent Cells Preserve Perineuronal Nets and Stimulate Neural Plasticity in ALS Rats. *Neuron* **2014**, *81*, 333–348. (b) Rabin, S. J.; Kim, J. M. H.; Baughn, M.; Libby, R. T.; Kim, Y. J.; Fan, Y.; Libby, R. T.; La Spada, A.; Stone, B.; Ravits, J. Sporadic ALS has compartment-specific aberrant exon splicing and perturbation of cell-matrix adhesion biology. *Hum. Mol. Genet.* **2010**, *19*, 313–328.
- (6) (a) Su, W.; Frohman, M. A. Phospholipase D. In *Handbook of Cell Signaling*, 2nd ed.; Bradshaw, R. A., Dennis, E. A., Eds.; Elsevier: New York, 2010; Vol. 1, pp 1167–1176. (b) Selvy, P. E.; Lavieri, R. R.; Lindsley, C. W.; Brown, H. A. Phospholipase D - enzymology, functionality, and chemical modulation. *Chem. Rev.* **2011**, *111*, 6064–6119.
- (7) (a) Ghosh, S.; Strum, J. C.; Sciorra, V. A.; Daniel, L.; Bell, R. M. Raf-1 kinase possesses distinct binding domains for phosphatidylserine and phosphatidic acid. Phosphatidic acid regulates the translocation of Raf-1 in 12-O-tetradecanoylphorbol-13-acetate-stimulated Madin-Darby canine kidney cells. *J. Biol. Chem.* **1996**, *271*, 8472–8480. (b) Rizzo, M. A.; Shome, K.; Watkins, S. C.; Romero, G. The recruitment of Raf-1 to membranes is mediated by direct interaction with phosphatidic acid and is independent of association with Ras. *J. Biol. Chem.* **2000**, *275*, 23911–23918. (c) Fang, Y.; Vilella-Bach, M.; Bachmann, R.; Flanigan, A.; Chen, J. Phosphatidic acid-mediated mitogenic activation of mTOR signaling. *Science* **2001**, *294*, 1942–1945.
- (8) Tanguy, E.; Wang, Q.; Moine, H.; Vitale, N. Phosphatidic Acid: From Pleiotropic Functions to Neuronal Pathology. *Front. Cell Neurosci.* **2019**, *13*, 2.
- (9) Brown, H. A.; Thomas, P. G.; Lindsley, C. W. Targeting phospholipase D in cancer, infection and neurodegenerative disorders. *Nat. Rev. Drug Disc.* **2017**, *16*, 351–367.
- (10) De Cuyper, H.; van Praag, H. M.; Verstraeten, D. The Clinical Significance of Halopemide, a Dopamine-Blocker Related to the Butyrophenones. *Neuropsychobiology* **1984**, *12*, 211–216. (b) Monovich, L.; Mugrage, B.; Quadros, E.; Toscano, K.; Tommasi, R.; LaVoie, S.; Liu, E.; Du, Z.; LaSala, D.; Boyar, W.; Steed, P. Optimization of halopemide for phospholipase D2 inhibition. *Bioorg. Med. Chem. Lett.* **2007**, *17*, 2310–2311.
- (11) (a) Waterson, A. G.; Scott, S. A.; Kett, N. R.; Blobaum, A. L.; Brown, A. B.; Lindsley, C. W. Isoform selective PLD inhibition by novel, chiral 2,8-diazaspiro[4.5]decan-1-one derivatives. *Bioorg. Med. Chem. Lett.* **2018**, *28*, 3670–3673. (b) Lewis, J. A.; Scott, S. A.; Lavieri, R.; Buck, J. R.; Selvy, P. E.; Stoops, S. L.; Armstrong, M. D.; Brown, H. A.; Lindsley, C. W. Design and synthesis of isoform-selective phospholipase D (PLD) inhibitors. Part I: Impact of alternative halogenated privileged structures for PLD1 specificity. *Bioorg. Med. Chem. Lett.* **2009**, *19*, 1916–1920. (c) Scott, S. A.; Selvy, P. E.; Buck, J. R.; Cho, H. P.; Criswell, T. L.; Thomas, A. L.; Armstrong, M. D.; Arteaga, C. L.; Lindsley, C. W.; Brown, H. A. Design of isoform-selective phospholipase D inhibitors that modulate cancer cell invasiveness. *Nat. Chem. Biol.* **2009**, *5*, 108–117.
- (d) Lavieri, R.; Scott, S. A.; Lewis, J. A.; Selvy, P. E.; Armstrong, M. D.; Brown, H. A.; Lindsley, C. W. Design and synthesis of isoform-selective phospholipase D (PLD) inhibitors. Part II. Identification of the 1,3,8-triazaspiro[4.5]decan-4-one privileged structure that engenders PLD2 selectivity. *Bioorg. Med. Chem. Lett.* **2009**, *19*, 2240–2243. (e) O'Reilly, M. C.; Scott, S. A.; Brown, K. A.; Oguin, T. H.; Thomas, P. G.; Daniels, J. S.; Morrison, R.; Brown, H. A.; Lindsley, C. W. Development of Dual PLD1/2 and PLD2 Selective Inhibitors from a Common 1,3,8-Triazaspiro[4.5]decan-4-one Core: Discovery of ML298 and ML299 That Decrease Invasive Migration in U87-MG Glioblastoma Cells. *J. Med. Chem.* **2013**, *56*, 2695–2696.
- (12)  $K_{pu,u}$  is the ratio of free compound concentration in the brain over the free compound concentration in the plasma at steady state, equation:  $K_{pu,u} = \frac{AUC_{brain,total}f_{u,brain}}{AUC_{plasma,total}f_{u,plasma}}$ . The  $K_{pu,u}$  values for 1 and 2 in mouse are 0.04 and 0.09, respectively, and the approximate  $K_{pu,u}$  of ML299 (3) was determined using the reported total brain/plasma ratio = 0.44 in ref 11e, using mouse plasma protein binding (%Fu = 8%) and brain binding (%Fu = 0.9%) values obtained at Biogen. This does not represent a steady-state  $K_{pu,u}$ .
- (13) The bacterial PLD structure has been reported; however, the human and bacterial proteins have low sequence conservation. Leiros, I.; Secundo, F.; Zambonelli, C.; Servi, S.; Hough, E. The first crystal structure of a phospholipase D. *Structure* **2000**, *8*, 655–667.
- (14) PLD1 activity was prioritized over its isoform PLD2, since PLD1 was found to be upregulated in human ALS patients (ref 5). PLD2 activity was monitored but not optimized during the investigation.
- (15) As full length PLD1/2 was not stable to isolation, the enzymatic activity of PLD1 and PLD2 were measured by immunoprecipitation of PLD1 from HEK-293 cell lysates. PLD was captured with a GTP antibody in an ELISA plate and 0.8.0 phosphatidyl choline was used as substrate; amplex red detection of choline was used as the readout. For a previously disclosure measurement of enzymatic activity of PLD; see ref 11c.
- (16) The cellular assay was measured in Calu-1 cells that express only PLD1 and not PLD2; the assay was a mass-spectrometry-based detection of  $d_9$ -phosphobutanol arising from PLD1-catalyzed transphosphatidylation with  $d_9$ -BuOH.<sup>11</sup>
- (17) Ghose, A. K.; Herberich, T.; Hudkins, R. L.; Dorsey, B. D.; Mallamo, J. P. Knowledge-Based, Central Nervous System (CNS) Lead Selection and Lead Optimization for CNS Drug Discovery. *ACS Chem. Neurosci.* **2012**, *3*, 50–68.
- (18) Metrick, C. M.; Peterson, E. A.; Santoro, J. C.; Enyedy, I. J.; Murugan, P.; Chen, T.; Michelsen, K.; Cullivan, M.; Spilker, K. A.; Kumar, P. R.; May-Dracka, T. L.; Chodaparambil, J. V. Human PLD structures enable drug design and characterization of isoenzyme selectivity. *Nat. Chem. Biol.* **2020**, *16*, 391–399.
- (19) Lovering, F.; Bikker, J.; Humblet, C. Escape from Flatland: Increasing Saturation as an Approach to Improving Clinical Success. *J. Med. Chem.* **2009**, *52*, 6752–6756.
- (20) See the SI for the full data table.
- (21) Bond, P. Phosphatidic acid: biosynthesis, pharmacokinetics, mechanisms of action and effect on strength and body composition in resistance-trained individuals. *Nutr. Metab. (Lond)* **2017**, *14*, 12.
- (22) (a) Morris, A. J.; Frohman, M. A.; Engebrecht, J. Measurement of phospholipase D activity. *Anal. Biochem.* **1997**, *252*, 1–9. (b) Brown, H. A.; Henage, L. G.; Preininger, A. M.; Xiang, Y.; Exton, J. H. Biochemical analysis of phospholipase D. *Methods Enzymol* **2007**, *434*, 49–87.
- (23) (a) Scott, S. A.; Xiang, Y.; Mathews, T. P.; Cho, H. P.; Myers, D. S.; Armstrong, M. D.; Tallman, K. A.; O'Reilly, M. C.; Lindsley, C. W.; Brown, H. A. Regulation of Phospholipase D Activity and Phosphatidic Acid Production after Purinergic (P2Y6) Receptor Stimulation. *J. Biol. Chem.* **2013**, *288*, 20477–20487. (b) Philip, F.; Ha, E. E.; Seeliger, M. A.; Frohman, M. A. Measuring Phospholipase D Enzymatic Activity Through Biochemical and Imaging Methods. *Methods Enzymol* **2017**, *583*, 309–325. (c) Oliveira, T. G.; Chan, R. B.; Tian, H.; Laredo, M.; Shui, G.; Staniszewski, A.; Zhang, H.; Wang,



L.; Kim, T.-W.; Duff, K. E.; Wenk, M. R.; Arancio, O.; Di Paolo, G. Phospholipase D2 Ablation Ameliorates Alzheimer's Disease-Linked Synaptic Dysfunction and Cognitive Deficits. *J. Neurosci.* **2010**, *30*, 16419–16428.

(24) Untargeted high-resolution LC-FT ICR-MS assay profiled the lipid pools and distinguished PtdBut species from the interference of other lipids in tissue. Chromatograms of PtdBut species were optimized to achieve characteristic LC elution profile. The targeted LC-MRM assay was also used to quantify each PtdBut species observed.